DALTON
FULL PAPER

# Structural characterisation, EPR and magnetic properties of f–f and f–d lanthanide(III) phenolic cryptates†

**Fernando Avecilla,[a] Carlos Platas-Iglesias,[a] Raquel Rodríguez-Cortiñas,[a] Geoffroy Guillemot,[b] Jean-Claude G. Bünzli,[b] Carlos D. Brondino,[c] Carlos F. G. C. Geraldes,[d] Andrés de Blas*[a] and Teresa Rodríguez-Blas*[a]**

[a] *Departamento de Química Fundamental, Universidade da Coruña, Campus da Zapateira s/n 15071 A Coruña, Spain. E-mail: mayter@mail.udc.es*
[b] *Institute of Molecular and Biological Chemistry, Swiss Federal Institute of Technology Lausanne, BCH 1402, CH-1015 Lausanne, Switzerland*
[c] *Facultad de Bioquímica y Ciencias Biológicas – U.N.L., Campus Universitario. Pje. El Pozo, CC 242. 3000 Santa Fe, Argentina*
[d] *Deparment of Biochemistry, FCT, University of Coimbra, 3001-4001 Coimbra, Portugal*

***Received 8th July 2002, Accepted 10th October 2002***
***First published as an Advance Article on the web 8th November 2002***

The Schiff base axial macrobicyclic ligand $L^1$ forms 4f–4f and 4f–3d cryptates with formula $[Gd_2(L^1 - 3H)(NO_3)_2](NO_3)\cdot 1.5H_2O$ (**1**), $[Tb_2(L^1 - 3H)(NO_3)_2](NO_3)\cdot 3EtOH\cdot H_2O$ (**2**), $[GdCu(L^1 - 3H)(NO_3)](NO_3)\cdot H_2O$ (**3**), $[LuCu(L^1 - 3H)(NO_3)](NO_3)\cdot H_2O$ (**4**) and $[GdZn(L^1 - 3H)(NO_3)](NO_3)\cdot H_2O$ (**5**). The macrobicyclic receptor $L^1$ is an azacryptand $N[(CH_2)_2N{=}CH{-}R{-}CH{=}N{-}(CH_2)_2]_3N$ (R =1,3-(2-OH-5-Me–$C_6H_2$)). The crystal structures of the five compounds have been determined by X-ray crystallography. The ligand is helically wrapped around the two metal ions, leading to pseudo-$C_3$ symmetries around the metals. In the solid state, the conformation of the cation in **1** and **2** is $\Lambda(\delta\delta\lambda)_5(\delta\delta\lambda)_5$ or its enantiomeric form $\Delta(\lambda\lambda\delta)_5(\lambda\lambda\delta)_5$, while in **3**, **4** and **5** it can be described as $\Lambda(\delta\delta\lambda)_5(\delta'\delta'\delta')_5$ (or $\Delta(\lambda\lambda\delta)_5(\lambda'\lambda'\lambda')_5$). In **1**, only one enantiomer is found in the crystal lattice, whereas in the other four compounds, both enantiomers are co-crystallised. The magnetic behaviour of the homodinuclear (Gd, Gd) and the heterodinuclear (Gd, Cu) cryptates points to a significant magnetic interaction between the two metal ions. This magnetic interaction is antiferromagnetic in the case of the Gd–Gd cryptate **1** ($J = -0.194(6)$ cm$^{-1}$), but ferromagnetic for the Gd–Cu one ($J = 2.2(1)$ cm$^{-1}$). The antiferromagnetic coupling observed for **1** is one of the largest ever reported. Although the ferromagnetic coupling observed for **3** is relatively weak, which is attributed to the strong bending of the bridging network, it is considerably stronger than the one reported for $[GdCu(L^2 - 3H)(DMF)](ClO_4)_2\cdot MeCN$. In spite of the similar coordination environment of the Gd(III) ion in compounds **1**, **3** and **5** their EPR spectra are different, thereby confirming the magnetic interactions between the Gd(III) ion and the Cu(II) ion in **3** and the other Gd(III) ion in **1**.

## Introduction

Lanthanide coordination compounds[1] are the subject of intense research efforts due to their applications as contrast agents for NMR imaging,[2,3] as catalysts in RNA hydrolysis,[4] as active agents in cancer radiotherapy,[5] or as luminescent stains for protein labelling and sensitive homogeneous immunoassays.[6] In recent years, an increasing interest has been devoted to the magnetic properties of dinuclear compounds[7] featuring simultaneously either 4f and 3d ions,[8–11] identical 4f ions[12–16] or even two different lanthanide (4f–4f′) ions,[17] since they can serve as models or precursors for novel magnetic materials, *e.g.* high-temperature superconducting ceramics. The simplicity of the magnetic properties of the Gd(III) ion facilitates examination of the 4f–3d and 4f–4f magnetic interactions in discrete dinuclear complexes. Magnetic interactions between a transition metal ion and Gd(III) are often found to be weakly ferromagnetic, with $J$ values typically smaller than 10 cm$^{-1}$, while they are usually weakly antiferromagnetic in Gd(III)–Gd(III) compounds. However, in a recent paper Costes *et al.*[10] demonstrated that antiferromagnetic interactions may also occur between the Cu(II)/Gd(III) couple. In a subsequent work,[12] the same authors have also found a ferromagnetic Gd(III)–Gd(III) interaction. It should be noted that the number of di- and poly-nuclear Gd(III) compounds for which structural and magnetic data are available is restricted and that the factors governing the Gd ··· Gd interaction have not been clarified. Therefore, to better understand the magnetic interactions between Cu(II)/Gd(III) and Gd(III)/Gd(III) couples the magnetic properties of new structurally characterized Gd–Gd or Gd–Cu compounds should be investigated.

Monometallic cryptates with $L^1$ and $L^3$ (Scheme 1) have been obtained for Ln = Sc, Y, Gd, Eu, Tb and Dy by transmetallation of the sodium derivatives.[18] In subsequent works, we have shown that the 1 : 1 cryptates $[LnL^1(NO_3)][Ln(NO_3)_5]\cdot xH_2O$ or $[LnL^1(NO_3)](NO_3)_2\cdot xH_2O$ (Ln = La–Lu) can be obtained by direct template reaction[19] and we have reported their structure in both the solid state and in aqueous solution[20,21] as well as their photophysical properties and relaxivity.[22] The corresponding anionic cryptand $(L^1 - 3H)^{3-}$ is also able to accommodate two lanthanide(III) ions into the macrobicyclic cavity and yield cryptates with formula $[Ln_2(L^1 - 3H)(NO_3)_2](NO_3)\cdot xH_2O\cdot yEtOH$ (Ln = Gd–Lu).[23] More recently, Luo *et al.* reported the first examples of 4f–3d cryptates with formula $[DyCu(L^2 - 3H)(DMF)](ClO_4)_2\cdot MeCN$[24] and $[GdNi(L^1 - 3H)(DMF)](ClO_4)_2\cdot MeCN$,[25] as well as the magnetic properties of

† Electronic supplementary information (ESI) available: tables of selected bond angles for cryptates **1**–**5**. See http://www.rsc.org/suppdata/dt/b2/b206615g/

 DOI: 10.1039/b206615g

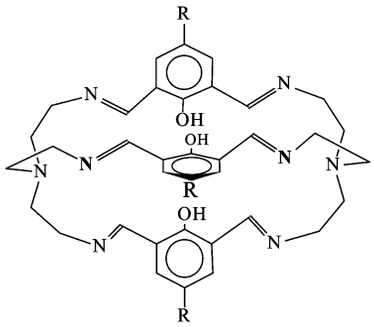

$L^1$: R = Me
$L^2$: R = Cl
$L^3$: R = *t*-Bu

**Scheme 1**

the Ni(II) derivative. In a recent work, we also demonstrated that $L^1$ forms Ln(III)–Zn(II) cryptates with formula $[LnZn(NO_3)(L^1 - 3H)](NO_3)\cdot xH_2O\cdot y$MeOH (Ln = Ce–Lu), and we have reported their solid state and solution structures, as well as their photophysical properties.[26]

Herein, we investigate the solid state structure, magnetic and EPR properties of 4f–4f and 4f–3d cryptates with formula $[Gd_2(L^1 - 3H)(NO_3)_2](NO_3)\cdot 1.5H_2O$ (**1**), $[Tb_2(L^1 - 3H)(NO_3)_2](NO_3)\cdot 3EtOH\cdot H_2O$ (**2**), $[GdCu(L^1 - 3H)(NO_3)](NO_3)\cdot H_2O$ (**3**) and $[LuCu(L^1 - 3H)(NO_3)](NO_3)\cdot H_2O$ (**4**) which possess $[LnO_3Ln]$ or $[CuO_3Ln]$ cores. To substantiate the discussion, the X-ray crystal structure of $[GdZn(L^1 - 3H)(NO_3)](NO_3)\cdot 0.5CH_3CN\cdot 0.5CH_3OH\cdot 1.5H_2O$ (**5**) is also reported. While our work was in progress, Luo *et al*. reported a ferromagnetic interaction in a Gd(III)–Cu(II) cryptate with formula $[GdCu(L^2 - 3H)(DMF)](ClO_4)_2\cdot$MeCN ($J = +0.68$ cm$^{-1}$, $g_{Cu} = g_{Gd} = 1.99$ and $R = 6.3 \times 10^{-4}$).[27] Although we also report here a ferromagnetic coupling for **3**, its magnitude is considerably larger as a consequence of small structural differences that drastically affect the magnetic properties in this family of compounds.

## Experimental

### Physicochemical measurements

Elemental analyses were carried out on a Carlo Erba 1180 elemental analyser and FAB mass spectra were recorded on a FISONS QUATRO mass spectrometer with a Cs ion-gun using 3-nitrobenzyl alcohol as matrix. IR-spectra were recorded, as KBr discs, using a Bruker Vector 22 spectrophotometer. EPR measurements were performed on a Bruker EMX spectrometer operating at the X-band and fitted with an Oxford Instrument liquid-helium flow cryostat. The EPR experiments were performed using either powdered samples or 1 mM solutions of the cryptates dissolved in acetonitrile. EPR simulations were performed with the program WIN-EPR SimFonia V.1.2 from Bruker Instruments, Inc. Magnetic susceptibility measurements (1.9–298 K) were made on a MPMS5 SQUID susceptometer from Quantum Design Inc. operating at a magnetic field strength of 1 kOe. Corrections for diamagnetism were made using Pascal constants.[28] The samples were prepared under a controlled atmosphere in a glove-box.

### Syntheses and characterisation

The lanthanide mononuclear cryptates $[GdL^1(NO_3)](NO_3)_2\cdot 2H_2O$ and $[LuL^1(NO_3)](NO_3)_2\cdot H_2O$[20] as well as the Gd–Zn(II) cryptate with formula $[GdZn(L^1 - 3H)(NO_3)](NO_3)\cdot H_2O$[26] (**5**) were prepared as previously described. Single crystals with formula $[GdZn(L^1 - 3H)(NO_3)](NO_3)\cdot 1.5H_2O\cdot 0.5$MeOH$\cdot 0.5CH_3CN$ were obtained by slow diffusion of diethyl ether into a solution of the cryptate in acetonitrile. Compound **1** was obtained by an identical procedure to that used for **2**[23] (yield 15%). [Found: C, 37.9; H, 4.3; N, 12.2. Calc. for $C_{39}H_{45}N_{11}O_{12}Gd_2\cdot 4H_2O$: C, 37.6; H, 4.3; N, 12.4%]. IR $\nu$(cm$^{-1}$, KBr) 1639 (HC=N), 1456, 1411, 1281, 1025, 810 ($NO_3^-$). FAB mass spectrum: *m*/*z* 1112 $[Gd_2(L^1 - 3H)(NO_3)_2]^+$. Crystals with formula $[Gd_2(L^1 - 3H)(NO_3)_2](NO_3)\cdot 1.5H_2O$ and $[Tb_2(L^1 - 3H)(NO_3)_2](NO_3)\cdot 3EtOH\cdot H_2O$ suitable for X-ray diffraction were grown from solutions of the cryptates in ethanol.

**$[GdCu(L^1 - 3H)(NO_3)](NO_3)\cdot H_2O$ (3).** 0.0097 g (0.22 mmol) of $CaH_2$ and 50 μL of DMF were added to a stirred solution of $[GdL^1(NO_3)](NO_3)_2\cdot 2H_2O$ (0.096 g; 0.091 mmol) in 20 cm$^3$ of absolute methanol. The resulting mixture was stirred for 48 h and then filtered. The filtrate was added to a solution of $Cu(NO_3)_2\cdot 3H_2O$ (0.022 g; 0.091 mmol) in 5 cm$^3$ of methanol, stirred and heated to reflux for 7 h and then concentrated to 5–10 cm$^3$ under vacuum. The cryptate was isolated as a red crystalline solid by slow diffusion of diethyl ether into this solution (yield 58%). [Found: C, 45.4; H, 4.4; N, 13.3. Calc. for $C_{39}CuGdH_{45}N_{10}O_9\cdot H_2O$: C, 45.4; H, 4.6; N, 13.6%]. $\Lambda_M$ (acetonitrile): 132 $\Omega^{-1}$ cm$^2$ mol$^{-1}$ (1 : 1 electrolyte). IR $\nu$(cm$^{-1}$, KBr) 1631 (HC=N), 1450, 1385, 1342, 1039 ($NO_3^-$). FAB mass spectrum: *m*/*z* 957 $[GdCu(L^1 - 3H)(NO_3)]^+$. Crystals of formula $[GdCu(L^1 - 3H)(NO_3)](NO_3)\cdot CH_3OH\cdot 2H_2O$ suitable for X-ray diffraction were grown by slow diffusion of diethyl ether into a solution of the cryptate in methanol.

**$[LuCu(L^1 - 3H)(NO_3)](NO_3)\cdot H_2O$ (4).** The red compound was prepared as described for **3** by using 0.104 g (0.097 mmol) of $[LuL^1(NO_3)](NO_3)_2\cdot H_2O$ (yield 59%). [Found: C, 44.8; H, 4.5; N, 12.9. Calc. for $C_{39}CuLuH_{45}N_{10}O_9\cdot H_2O$: C, 44.4; H, 4.5; N, 13.3%]. $\Lambda_M$ (acetonitrile): 148 $\Omega^{-1}$ cm$^2$ mol$^{-1}$ (1 : 1 electrolyte). IR $\nu$(cm$^{-1}$, KBr) 1634 (HC=N), 1456, 1385, 1341, ($NO_3^-$). FAB mass spectrum: *m*/*z* 973 $[LuCu(L^1 - 3H)(NO_3)]^+$. Crystals of formula $[LuCu(L^1 - 3H)(NO_3)](NO_3)\cdot 2CH_3OH\cdot H_2O$ suitable for X-ray diffraction were grown by slow diffusion of diethyl ether into a solution of the cryptate in methanol.

### X-Ray crystal structure determinations

Three dimensional X-ray data were collected on Siemens Smart 1000 CCD (**1**, **3**, **4** and **5**) or Bruker Smart 1000 CCD instruments (**2**). Complex scattering factors were taken from the program package SHELXTL.[29] For **1**, the absolute configuration has been established by refinement of the enantiomorph polarity parameter [$x = -0.02(2)$].[30] The structure of **1** and **2** present disorders of the ionic nitrates. These disorders have been resolved and several atomic sites have been observed and refined with anisotropic atomic displacement parameters. The site occupancy factors for N(11A), O(10A), O(11A) and O(12A) were 0.44440 for **1** and 0.62084 for **2**. Crystal data and details on data collection and refinement are summarised in Table 1.

CCDC reference numbers 189517–189521.

See http://www.rsc.org/suppdata/dt/b2/b206615g/ for crystallograhic data in CIF or other electronic format.

## Results and discussion

### Structural characterisation of the cryptates in the solid state

The X-ray crystal structures of these binuclear cryptates confirm the presence of both metal ions encapsulated into the macrobicyclic cavity. The crystals of **1** and **2** consist of $[Ln_2(L^1 - 3H)(NO_3)_2]^+$ cations (Ln = Gd, Tb) and an independent nitrate anion, whereas crystals of **3**, **4** and **5** consist of the cations $[LnM(L^1 - 3H)(NO_3)]^+$ (Ln/M = Gd/Cu, Lu/Cu, Gd/Zn) and one well separated nitrate anion. All the crystal lattices also contain solvent and/or water molecules. Bond lengths are summarised in Tables 2 and 3. Tables S1, S2 and S3 (ESI) list

**Table 1** Crystal data and structure refinement for **1**–**5**

| | **1** | **2** | **3** | **4** | **5** |
|---|---|---|---|---|---|
| Formula | $C_{39}H_{48}Gd_2N_{11}O_{13.5}$ | $C_{45}H_{65}N_{11}O_{16}Tb_2$ | $C_{40}H_{53}CuGdN_{10}O_{12}$ | $C_{41}H_{55}CuLuN_{10}O_{12}$ | $C_{40.5}H_{51.5}GdN_{10.5}O_{11}$ Zn |
| Molecular weight | 1201.38 | 1333.92 | 1086.71 | 1118.46 | 1084.04 |
| Crystal system | Tetragonal | Tetragonal | Monoclinic | Monoclinic | Triclinic |
| Space group | $P4_12_12$ | $I4_1/a$ | $C2/c$ | $C2/c$ | $P\bar{1}$ |
| $T$/K | 193(2) | 150(2) | 173(2) | 173(2) | 173(2) |
| $a$/Å | 17.715(4) | 28.2130(17) | 33.359(3) | 33.067(9) | 10.7705(14) |
| $b$/Å | 17.715(4) | 28.2130(17) | 11.0095(9) | 11.035(3) | 12.6590(16) |
| $c$/Å | 29.3028(4) | 30.107(3) | 25.614(2) | 25.516(7) | 17.494(2) |
| $\alpha$/° | 90 | 90 | 90 | 90 | 81.937(3) |
| $\beta$/° | 90 | 90 | 104.550(2) | 104.098(5) | 87.968(3) |
| $\gamma$/° | 90 | 90 | 90 | 90 | 81.534(2) |
| $V$/Å$^3$ | 9196.3(3) | 23965(3) | 9105.3(13) | 9030(4) | 2335.6(5) |
| $F_{000}$ | 4760 | 10720 | 4416 | 4536 | 1100 |
| $Z$ | 8 | 16 | 8 | 8 | 2 |
| $D_{calc}$/g cm$^{-3}$ | 1.736 | 1.479 | 1.585 | 1.645 | 1.541 |
| $\mu$/mm$^{-1}$ | 2.935 | 2.410 | 1.982 | 2.717 | 1.988 |
| $R_{int}$ | 0.1351 | 0.0843 | 0.1087 | 0.0438 | 0.0732 |
| Reflections measured | 63833 | 78945 | 28136 | 31518 | 14743 |
| Reflections observed | 7953 | 10010 | 5722 | 8942 | 4801 |
| Goodness-of-fit on $F^2$ | 1.065 | 1.094 | 0.981 | 1.034 | 0.945 |
| $R_1$ | 0.0654 | 0.0608 | 0.0581 | 0.0351 | 0.0788 |
| $wR_2$ (all data) | 0.1706 | 0.2017 | 0.1693 | 0.0915 | 0.1777 |

$R_1 = \Sigma||F_o| - |F_c||/\Sigma|F_o|$. $wR_2 = \{\Sigma[w(|F_o|^2 - |F_c|^2)^2]/\Sigma[w(F_o^4)]\}^{1/2}$.

**Table 2** Selected bond lengths (Å) for cryptates **1** and **2**

| | **1** | **2** | | **1** | **2** |
|---|---|---|---|---|---|
| Ln(1)–O(4) | 2.317(7) | 2.310(5) | Ln(2)–O(6) | 2.344(7) | 2.301(5) |
| Ln(1)–O(5) | 2.397(7) | 2.402(5) | Ln(2)–O(4) | 2.433(8) | 2.421(5) |
| Ln(1)–O(6) | 2.400(8) | 2.424(5) | Ln(2)–O(5) | 2.432(7) | 2.436(5) |
| Ln(1)–N(6) | 2.436(10) | 2.460(6) | Ln(2)–N(2) | 2.456(9) | 2.452(6) |
| Ln(1)–N(7) | 2.499(10) | 2.463(6) | Ln(2)–O(8) | 2.466(10) | 2.457(6) |
| Ln(1)–O(3) | 2.498(8) | 2.491(5) | Ln(2)–N(3) | 2.504(10) | 2.524(6) |
| Ln(1)–N(5) | 2.509(9) | 2.496(5) | Ln(2)–N(4) | 2.504(11) | 2.459(6) |
| Ln(1)–N(8) | 2.667(9) | 2.680(6) | Ln(2)–N(1) | 2.648(9) | 2.648(7) |
| Ln(1)–O(2) | 2.773(9) | 2.635(6) | Ln(2)–O(7) | 2.705(14) | 2.638(6) |

**Table 3** Selected bond lengths (Å) for cryptates **3**, **4** and **5**

| | **3** | **4** | **5** |
|---|---|---|---|
| Ln(1)–O(5) | 2.243(5) | 2.326(2) | 2.286(6) |
| Ln(1)–O(4) | 2.336(5) | 2.185(2) | 2.276(6) |
| Ln(1)–O(6) | 2.383(5) | 2.271(2) | 2.337(6) |
| Ln(1)–O(3) | 2.442(6) | 2.341(2) | 2.470(7) |
| Ln(1)–N(6) | 2.475(7) | 2.476(3) | 2.525(9) |
| Ln(1)–N(5) | 2.483(6) | 2.412(3) | 2.525(8) |
| Ln(1)–N(7) | 2.522(7) | 2.406(3) | 2.501(8) |
| Ln(1)–N(8) | 2.646(6) | 2.595(3) | 2.604(8) |
| M$^{II}$(1)–O(4) | 1.979(5) | 2.286(3) | 2.321(6) |
| M$^{II}$(1)–N(4) | 2.007(6) | 2.182(3) | 2.062(8) |
| M$^{II}$(1)–N(3) | 2.104(7) | 2.006(3) | 2.130(8) |
| M$^{II}$(1)–N(2) | 2.157(7) | 2.091(3) | 2.105(8) |
| M$^{II}$(1)–O(6) | 2.237(5) | 1.968(2) | 2.210(6) |
| M$^{II}$(1)–O(5) | 2.291(5) | 2.209(2) | 2.121(6) |

selected angles for metal coordination environments. Fig. 1 displays a view of complexes $[Ln_2(L^1 - 3H)(NO_3)_2]^+$ (Ln = Gd, Tb); each lanthanide(III) ion is co-ordinated by the three phenolate oxygen atoms, three imine nitrogen atoms and one bridgehead nitrogen atom, as well as one nitrate group in a bidentate fashion.

Figs. 2 and 3 display a view of complexes $[LnM(L^1 - 3H)(NO_3)]^+$ (Ln/M = Gd/Cu, Lu/Cu, Gd/Zn); when one of the lanthanide(III) ions present in **1** and **2** is replaced by a d-block metal ion, Cu(II) or Zn(II), the coordination environment around the Ln(III) ion does not change significantly, except for the fact that one nitrate anion coordinates now in a monodentate fashion. The d-block metal ion is hexacoordinated being only bound to the three μ-phenolate oxygen atoms and the other three imino-nitrogen atoms. The M–bridgehead nitrogen atom distance is too long to be considered a bond distance. The presence of the phenolate groups allows the two guest metal ions to be situated close to each other, with Ln(III)–Ln(III) distances of 3.5006(8) for **1** and 3.5080(5) Å for **2**, and Ln(III)–M(II) distances of 3.2454(10) (**3**), 3.2221(9) (**4**) and 3.2941(13) Å (**5**). The distances Ln(III)–Cu(II) are similar to the Dy(III)–Cu(II) distance reported for $[DyCu(L^2 - 3H)(DMF)](ClO_4)_2 \cdot MeCN$ (3.255 Å).[24]

In the homobinuclear Ln–Ln cryptates, the Ln(2) ion lies 0.9074 (**1**) and 0.9161 (**2**) Å below the plane formed by N(2), N(3), N(4) and O(8) (deviation from planarity 0.0376 and 0.0328 Å, respectively), while the Ln(1) ion lies 0.9092 (**1**) and 0.9360 (**2**) Å over the plane formed by N(5), N(6), N(7) and O(3) (deviation from planarity 0.0475 and 0.0196 Å, respectively). In the heterobinuclear cryptates, the lanthanide(III) ion lies 0.8588 (**3**), 0.8278 (**4**) and 0.8728 (**5**) Å above the plane formed by N(5), N(6), N(7) and O(3), and 1.7244 (**3**), 1.6796 (**4**) and 1.7009 Å (**5**) below the plane defined by the three μ-phenolate oxygen atoms. The d-block metal ion is located 0.9938 (**3**), 1.0050 (**4**) and 0.9430 Å (**5**) below the plane defined by the three azomethine nitrogen atoms N(2), N(3) and N(4), and 1.5059 (**3**), 1.5265 (**4**) and 1.5883 Å (**5**) above the plane defined by the three μ-phenolate oxygen atoms. In the five cryptates, the bond distance between the corresponding Ln(III) ion and the bridgehead nitrogen atom is considerably longer than those between the Ln(III) ion and the imino-nitrogen atoms, pointing to a weak interaction between the amine nitrogen atom and the lanthanide ions. As previously observed for the Dy(III)–Dy(III) analogue,[22] the coordination polyhedron around each metal ion in **1** and **2** can be best described as a monocapped distorted dodecahedron, where an oxygen atom

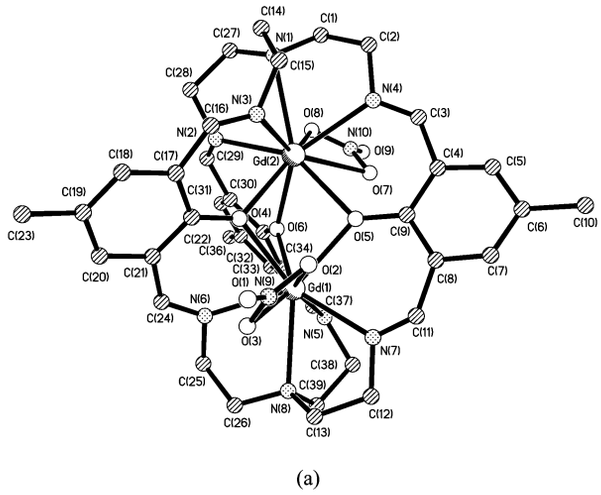


(a)

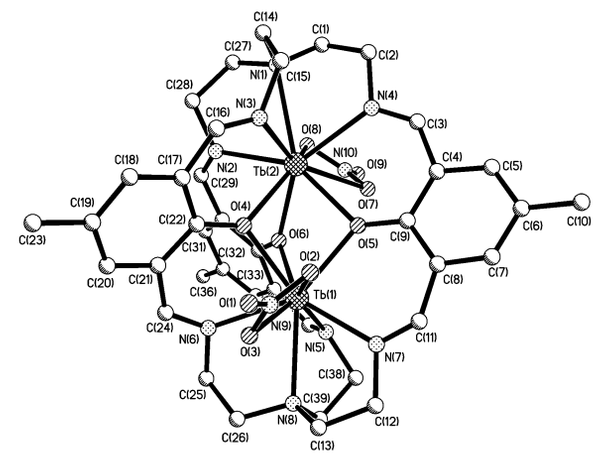


(b)

**Fig. 1** X-Ray crystal structure of $[Ln_2(L^1 - 3H)(NO_3)_2]^+$ (Ln = Gd, (a); Ln = Tb, (b)). Hydrogen atoms are omitted for clarity.

of the bidentate nitrate group occupies the capping position. However, the Ln(III) ion in **3**, **4** and **5** is eight coordinate, and the coordination polyhedron around the metal ion can be best described as a distorted dodecahedron. The coordination polyhedron around the Cu(II) or Zn(II) ions in **3**, **4** and **5** can be depicted as a severely distorted octahedron. The two triangular faces defined by the three phenolate oxygen atoms (O(4), O(5) and O(6)) and by the three imine nitrogen atoms (N(2), N(3) and N(4)) maintain a nearly parallel arrangement, with angles of 4.7 (**3**), 4.5 (**4**) and 3.1° (**5**); the mean twist angles between these triangular faces amount to 43.9 (**3**), 43.2 (**4**) and 40.7° (**5**), indicating an important distortion of the polyhedron from an octahedron (ideal value 60°) toward a trigonal prism (ideal value 0°), in agreement with the EPR data (*vide infra*). This distorted polyhedron shares the triangular face described by the three phenolate oxygen atoms with the polyhedron around the Ln(III) ion (Fig. 4).

In our cryptates the anionic macrobicyclic receptor $(L^1 - 3H)^{3-}$ adopts a *sss endo-endo* conformation, with the nitrogen atoms of the imine bonds pointing at the same side of the aromatic ring in the three chains and the N(1) and N(8) lone pairs directed towards the central cavity.[22] The receptor $(L^1 - 3H)^{3-}$ is twisted around the N(1)–N(8) axis in the five cryptates generating triple helical structures that, in turn, induce structural chirality in this family of compounds, as we previously described.[26] The cavity of the cryptand may be viewed as a trigonal antiprism defined by the six azomethine nitrogen atoms. The upper and lower triangular faces of the antiprism are connected by the three N=CH–R–CH=N (R = 1,3-(2-OH-5-Me-$C_6H_2$)) units (see Fig. 5), generating two possible helical

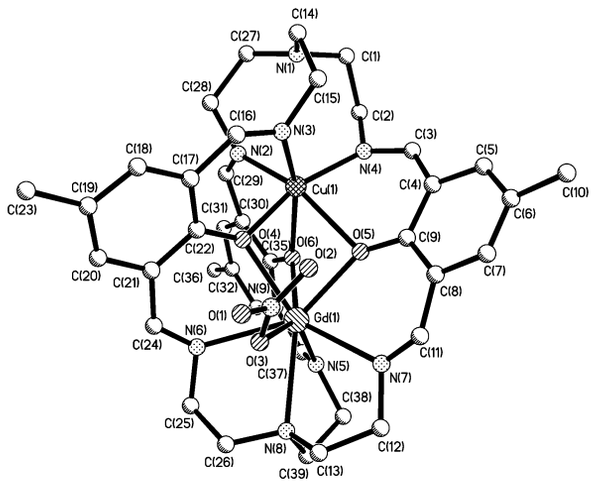


(a)

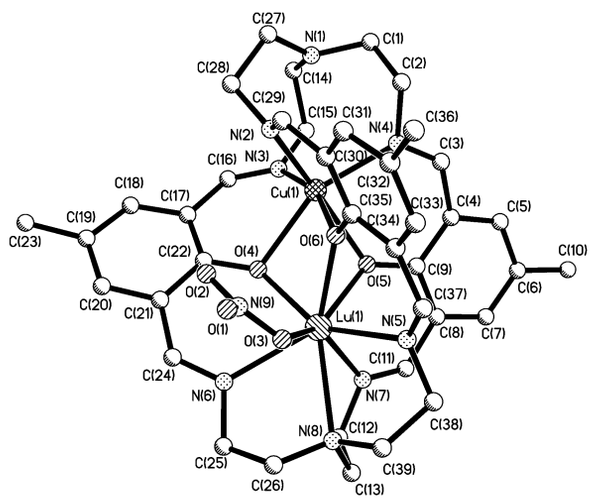


(b)

**Fig. 2** X-Ray crystal structure of $[LnCu(L^1 - 3H)(NO_3)]^+$ (Ln = Gd, (a); Ln = Lu, (b)). Hydrogen atoms are omitted for clarity.

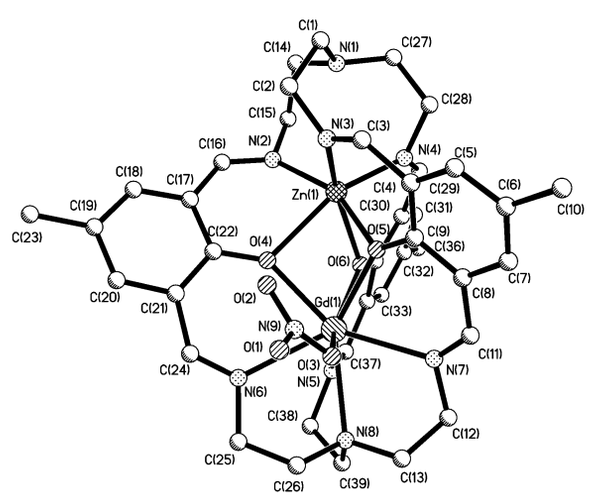


**Fig. 3** X-Ray crystal structure of $[GdZn(L^1 - 3H)(NO_3)]^+$. Hydrogen atoms are omitted for clarity.

structures corresponding to two different optical isomers that can be labelled as Λ or Δ, indicating either *left-handed* (Λ) or *right-handed* (Δ) structural chirality about the pseudo-three-fold symmetry axis of the complex.

Likewise, the coordinated $N^a$–$[(CH_2)$–$N^i]_3$ units of one side of the cavity of the macrobicyclic receptor $(L^1 - 3H)^{3-}$ (where

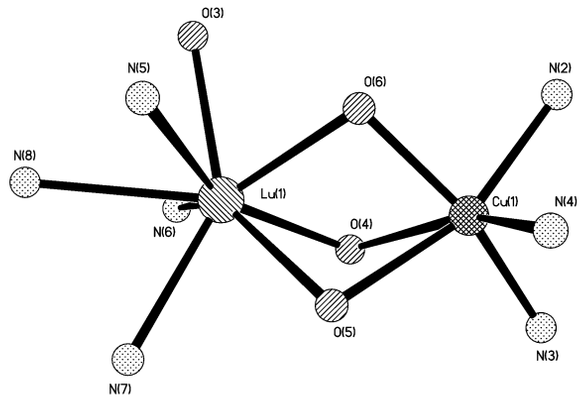


**Fig. 4** View of the coordination polyhedron in $[LuCu(L^1 - 3H)(NO_3)]^+$.

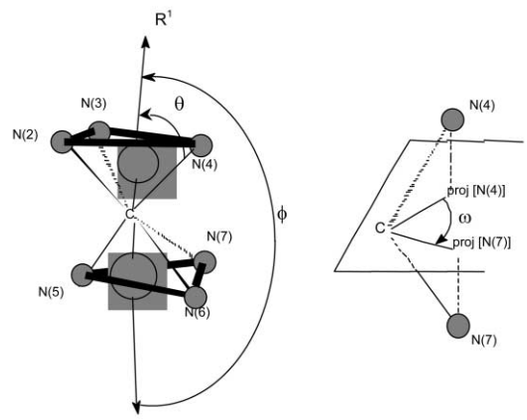


**Fig. 5** Definition of the angles and vectors used in the analysis of helical structure in compounds **1**–**5**.

$N^a$ and $N^i$ denote the amine and imine nitrogen atoms respectively) form three five-membered chelate rings $\overbrace{Ln–N^a–C–C–N^i}$, which adopt conformations that can be described as $(\delta\delta\lambda)_5$ or $(\lambda\lambda\delta)_5$. Moreover, the five membered pseudo-chelate rings $\overbrace{Cu–N^i–C–C–N^a}$ in **3** and **4** or $\overbrace{Zn–N^i–C–C–N^a}$ in **5** adopt $(\delta\delta\delta)_5$ or $(\lambda\lambda\lambda)_5$ conformations. In the following, we will use the notations $\delta'$ and $\lambda'$ for the two enantiomeric forms of the five membered pseudo-chelate rings when the metal ion is Cu(II) or Zn(II). Therefore, the conformation of the chelate rings in **3**, **4** and **5** can be described as $(\delta\delta\lambda)_5(\delta'\delta'\delta')_5$ or $(\lambda\lambda\delta)_5(\lambda'\lambda'\lambda')_5$. Inspection of the crystal structure data reveals that in **3**, **4** and **5** two $\Lambda(\delta\delta\lambda)_5(\delta'\delta'\delta')_5$ and $\Delta(\lambda\lambda\delta)_5(\lambda'\lambda'\lambda')_5$ enantiomers co-crystallize in equal amounts (racemate). Compound **2** also crystallises as a racemic mixture of enantiomers $\Lambda(\delta\delta\lambda)_5(\delta\delta\lambda)_5$ (or $\Delta(\lambda\lambda\delta)_5(\lambda\lambda\delta)_5$). However, compound **1** crystallises in a chiral space group, and only one $\Delta(\lambda\lambda\delta)_5(\lambda\lambda\delta)_5$ enantiomer is found in the X-ray structure. This $(\lambda\lambda\delta)_5$ or $(\delta\delta\lambda)_5$ "conformational mixture" is probably induced by the presence, in the solid state, of a relatively bulky nitrate anion between two chains of the ligand inducing an energetically less favourable symmetric $(\lambda\lambda\lambda)_5$ (or $(\delta\delta\delta)_5$) conformation compared with the asymmetric $(\lambda\lambda\delta)_5$ (or $(\delta\delta\lambda)_5$) one.

To determine the degree of torsion of the helix around the pseudo $C_3$ axis, as well as its degree of distortion from $C_3$ symmetry, we have performed a geometric analysis of the trigonal antiprism based on the determination of three angles, $\phi$, $\theta_i$, and $\omega_i$ (Fig. 5).[26,31] The average bending of the helical structure is measured by the angle $\phi$ between the sum vectors $R_1$ and $R_2$ ($R_1 = \Sigma_j\, C - N(j)$, $j = 2$, 3 and 4; $R_2 = \Sigma_j\, C - N(j)$, $j = 5$, 6 and 7; $\phi = 180°$ for an ideal $C_3$ symmetry and $C$ is a centroid placed in the axis containing both metal ions at an equal distance from each of them). The angles $\theta_i$ reflect the flattening of the helical structure along the pseudo-$C_3$ axis, defined as $R_2 - R_1$. Finally, the angles $\omega_i$ show how much the helix twists along the pseudo-$C_3$ axis. In the five helical structures, the $\phi$ angles do not deviate much from the expected value of 180° for a symmetrical helix, indicating a small bending of the triple helix along the pseudo-$C_3$ axis (Table 4). The flattening of the helix along the pseudo-$C_3$ axis is very similar for the five cryptates, in spite of the larger ionic radius of Gd(III) and Lu(III) compared to those of Cu(II) and Zn(II). The analysis of the angles $\omega_i$ show that the individual values do deviate significantly from the mean value, reflecting an important distortion of the helices. This distortion is more important for cryptates **1** and **2**, which is also reflected in the large $\alpha$ angles between the upper and lower facial planes described by the imine nitrogen atoms in these structures (Table 4). The helical structure is on average slightly more twisted in compounds **3** and **4** than in **1** and **2** and **5** (Table 4).

## Magnetic properties

**Magnetic properties of 1 and 2.** The magnetic behaviour of compound **1** is represented in Fig. 6 in the form of the thermal

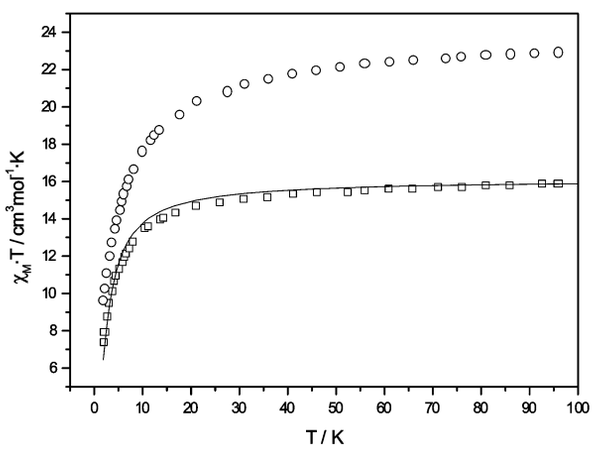


**Fig. 6** Temperature dependence of the $\chi_M T$ product for cryptates **1** (squares) and **2** (circles). The solid lines represent the best fit of the experimental data as discussed in the text.

dependence of the $\chi_M T$ product. At 100 K, $\chi_M T$ is equal to 15.9 $cm^3$ K $mol^{-1}$, which corresponds closely to the value expected for two non-interacting gadolinium ions (15.8 $cm^3$ K $mol^{-1}$). On lowering the temperature $\chi_M T$ decreases reaching a value of 7.42 $cm^3$ K $mol^{-1}$ at 1.88 K. The resulting profile is indicative of an antiferromagnetic interaction. A quantitative analysis can be performed on the basis of a spin only expression derived from the isotropic spin Hamiltonian $H = -JS_{Gd1}\cdot S_{Gd2}$ with quantum numbers $S_{Gd1} = S_{Gd2} = 7/2$ (eqn. (1)):[32]

$$\chi_M T = \frac{2N\beta^2 g^2}{k} \times \left( \frac{e^x + 5e^{3x} + 14e^{6x} + 30e^{10x} + 55e^{15x} + 91e^{21x} + 140e^{28x}}{1 + 3e^x + 5e^{3x} + 7e^{6x} + 9e^{10x} + 11e^{15x} + 13e^{21x} + 15e^{28x}} \right) \quad (1)$$

with

$$x = J/kT \quad (2)$$

The best fit of the experimental data is obtained for $J = -0.194(6)$, $g = 2.023(5)$ and $R = 8.0 \times 10^{-4}$ ($R = \Sigma(\chi_{obs}T - \chi_{calc}T)^2/\Sigma(\chi_{obs}T)^2$ where $\chi_{calc}$ and $\chi_{obs}$ denote the calculated and observed molar magnetic susceptibilities, respectively). The antiferromagnetic nature of the interacting Gd(III) ions in **1** is consistent with those reported for other systems, for which $J$ values varying from $-0.045$ to $-0.211$ $cm^{-1}$ have been reported by using the isotropic spin Hamiltonian $\boldsymbol{H} = -JS_{Gd1}S_{Gd2}$.[17,32–36] The value observed for **1** is one of the largest ones reported so far. However, a correlation between the

**Table 4** Geometric analysis of the helical structures in $[Ln_2(L^1 - 3H)(NO_3)_2]^+$ (Ln = Gd, **1**; Tb, **2**), $[LnCu(L^1 - 3H)(NO_3)]^+$ (Ln = Gd, **3**; Lu, **4**) $[GdZn(L^1 - 3H)(NO_3)]^+$ (**5**)

| | **1** | **2** | **3** | **4** | **5** |
|---|---|---|---|---|---|
| $\alpha$ [a]/° | 17.1 | 16.9 | 5.1 | 5.9 | 5.9 |
| $\phi$/° | 177.8 | 175.5 | 171.4 | 170.1 | 170.0 |
| Mean $\theta_{\text{vsi-R1}}$ [b]/° | 39.2(7.5) | 38.9(8.3) | 33.7(1.5) | 33.9(0.3) | 35.9(0.6) |
| mean $\theta_{\text{vii-R2}}$ [b]/° | 41.0(8.0) | 38.9(7.7) | 43.0(7.0) | 42.5(9.5) | 41.2(7.9) |
| $\omega_i$ | 45.3 | 43.6 | 62.1 | 59.9 | 53.8 |
| | 68.1 | 67.6 | 69.7 | 61.5 | 60.2 |
| | 72.2 | 68.0 | 82.5 | 82.5 | 75.2 |
| Mean $\omega_i$ | 61.9 | 59.7 | 71.4 | 68.0 | 63.1 |

[a] Angle between the two triangular faces described by N(2), N(3) and N(4) (upper plane) and N(5), N(6) and N(7) (lower plane). [b] Standard deviations are given in parentheses.

magnetic properties and the structure of the compound is difficult because of the limited number of compounds of this type investigated to date.

Since for compound **2** the $^7F_6$ ground state of the Tb(III) ion has a first-order angular momentum, the magnetic properties of the Tb–Tb couple are not amenable to a simple analysis based on a spin Hamiltonian comprising only isotropic exchange. At 273.5 K, $\chi_M T$ is 23.3 cm$^3$ K mol$^{-1}$, which is close to the value predicted by the Van Vleck equation (23.6 cm$^3$ K mol$^{-1}$). Lowering the temperature causes $\chi_M T$ to decrease (Fig. 6), reaching a value of 9.6 cm$^3$ K mol$^{-1}$ at 1.9 K. This decrease in $\chi_M T$ could arise from a selective depopulation of excited crystal field states. Unfortunately, a quantitative analysis of the magnetic behaviour of **3** in order to determine whether or not a magnetic interaction takes place between the two Tb(III) ions is presently out of reach.

**Magnetic properties of 3 and 4.** As the Lu(III) ion is diamagnetic, compound **4** presents the expected magnetic behaviour for an isolated Cu(II) compound. The plot of $\chi_M$ *vs.* $1/T$ follows the Curie law ($g_{Cu} = 2.160(3)$, $R^2 > 0.9999$) and $\chi_M T$ remains constant and equal to 0.37 cm$^3$ K mol$^{-1}$ (within experimental error) in the temperature range 298–1.92 K. This is not the case for **3**, whose temperature dependence of the magnetic susceptibility is shown in Fig. 7 under the $\chi_M T$ *vs.* $T$

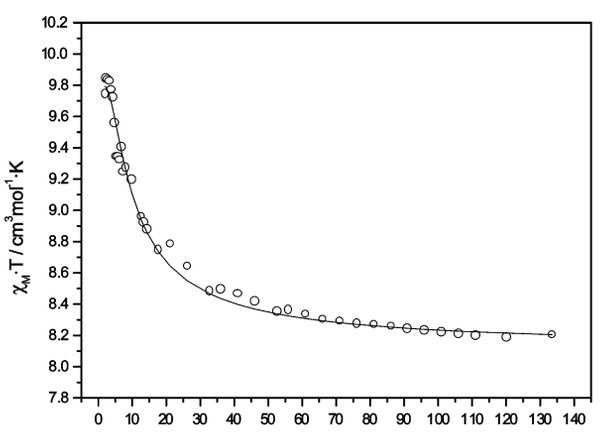


**Fig. 7** Temperature dependence of the $\chi_M T$ product for cryptate **3**. The solid line represents the best fit of the experimental data as discussed in the text.

form. At 280.1 K, $\chi_M T$ is 8.08 cm$^3$ K mol$^{-1}$, which is close to the spin-only value calculated assuming that there is no magnetic interaction between Cu(II) ($S_{Cu}$ = 1/2) and Gd(III) ($S_{Gd}$ = 7/2). Lowering the temperature causes $\chi_M T$ to increase, reaching a value of 9.8 cm$^3$ K mol$^{-1}$ at 2.2 K.

A quantitative analysis can be performed on the basis of a spin-only expression derived from a spin Hamiltonian $H = -JS_{Cu}\cdot S_{Gd}$. Keeping under consideration that the two low-lying levels $E_{(4)} = 0$ and and $E_{(3)} = 4J$ may have different $g$-values, $g_4 = (7g_{Gd} + g_{Cu})/8$ and $g_3 = (9g_{Gd} - g_{Cu})/8$, the following expression may be used (eqn. (3)):[9]

$$\chi_M T = \frac{4N\beta^2}{k}\left[\frac{15g_4^2 + 7g_3^2 e^{-4J/kT}}{9 + 7e^{-4J/kT}}\right] \quad (3)$$

where the symbols have their usual meaning. The best fit of the experimental data was obtained for $J = 2.2(1)$ cm$^{-1}$, $g_{Cu}$ = 1.93(4), $g_{Gd}$ = 1.986(3) and $R = 5.5 \times 10^{-5}$. Thus, a ferromagnetic spin–spin interaction between Cu(II) and Gd(III) appears to operate in **3**. A similar behaviour was observed for Gd–Cu compounds having ($CuO_2Gd$) bridging networks, the two oxygen donors being identical and afforded by either phenolato, acetonato or acetato groups.[37] While our work was in progress, a weaker ferromagnetic interaction ($J = 0.68$ cm$^{-1}$, $g_{Cu} = g_{Gd} = 1.99$ and $R = 6.3 \times 10^{-4}$) was reported by Luo *et al.*[27] for a similar Gd(III)–Cu(II) cryptate, $[GdCu(L^2 - 3H)(DMF)](ClO_4)_2\cdot MeCN$. However, the $g_{Cu}$ value that we report here for **3** ($g_{Cu}$ = 1.93(4)) is substantially lower than the one reported by Luo *et al.* ($g_{Cu}$ = 1.99). In order to check if these different $g_{Cu}$ values affect the calculated $J$ we have fitted our experimental data by fixing $g_{Cu} = g_{Gd} = 1.99$, obtaining $J = 1.85$ cm$^{-1}$. These data appear to confirm a substantially enhanced ferromagnetic interaction in **3** compared to $[GdCu(L^2 - 3H)(DMF)](ClO_4)_2\cdot MeCN$.

The stabilisation of the $S = 4$ state in these systems has been attributed to the coupling between the Gd(III)–Cu(II) ground configuration and the Gd(II)–Cu(III) excited configuration in which an electron has been transferred from the singly occupied 3d copper orbital to an empty 5d gadolinium orbital.[38] In such a mechanism, $J$ is given by eqn. (4):

$$J = \sum_{i=1}^{5}\left[\beta_{5d-3d}^2 \Delta / 4U^2 - \Delta^2)\right]_i \quad (4)$$

where $\beta_{5d-3d}$ is the transfer integral involving the singly-occupied copper orbital and a 5d gadolinium orbital, $\Delta$ is the energy gap between $S = 3$ and $S = 4$ excited states arising from the $4f^75d^1$ electron-transfer configuration, and $U$ is the energy cost of such a transfer. The summation applies for the five 5d orbitals. It has been observed that the bending of the bridging network in compounds having ($CuO_2Gd$) cores results in a depressed magnetic interaction, which has been attributed to a decrease of the $\beta_{5d-3d}$ integrals. Recently, a correlation between the absolute value of the ferromagnetic coupling constant $J$ and the dihedral angle $c$ has been proposed for compounds having ($CuO_2Gd$) cores (eqn. (5)):[9]

$$|J| = A\exp(Bc) \quad (5)$$

with $A = 11.5$, $B = -0.054$, $|J|$ in cm$^{-1}$, and $c$ in degrees. From the X-ray crystal structure of **3** we find dihedral angles $c$ of 36.1, 60.4 and 55.2° (calculated as the angle between a plane formed by two bridging oxygen atoms and the Cu(II) ion and that defined by the same two oxygen atoms and the Gd(III) ion).

These data clearly explain the weak magnetic interaction found in **3**, and much stronger ferromagnetic interactions were found for compounds with smaller dihedral angles.[9] From the X-ray structure of $[EuCu(L^2 - 3H)(DMF)](ClO_4)_2 \cdot MeCN$[27] we find dihedral angles *c* between the two halves (OCuO and OGdO) of 45.3, 52.4 and 55.7°. These structural data indicate that the stronger ferromagnetic coupling observed for **3** compared to that reported for the cryptate with $(L^2 - 3H)$ may be related with the different dihedral angles observed in the solid state structures. If so, small changes in the dihedral angles *c* could drastically affect the magnetic interactions in Gd(III)–Cu(II) compounds with $[CuO_3Gd]$ cores. The difference in the dihedral angles *c* between $[EuCu(L^2 - 3H)(DMF)](ClO_4)_2 \cdot MeCN$ and **3** can be attributed to the presence in the latter of a relatively bulky nitrate anion coordinated to the Gd(III) ion, which induces a more important distortion of the helical structure and, consequently, a decrease in one of the *c* angles. This opens new prespectives for the preparation of Gd(III)–Cu(II) compounds with more effective magnetic interactions, *e.g.* the replacement of the nitrate by a more bulky mono- or bi-dentate anion could result in a stronger distortion of the structure.

## EPR properties

**Compound 4.** Fig. 8A shows the EPR spectrum for a polycrystalline sample of **4**, which arises exclusively from the Cu(II) ion since Lu(III) is diamagnetic. The solution spectrum of **4** (not shown) is essentially identical to that observed in the solid state indicating that the structure of the metallic cluster is retained in solution.

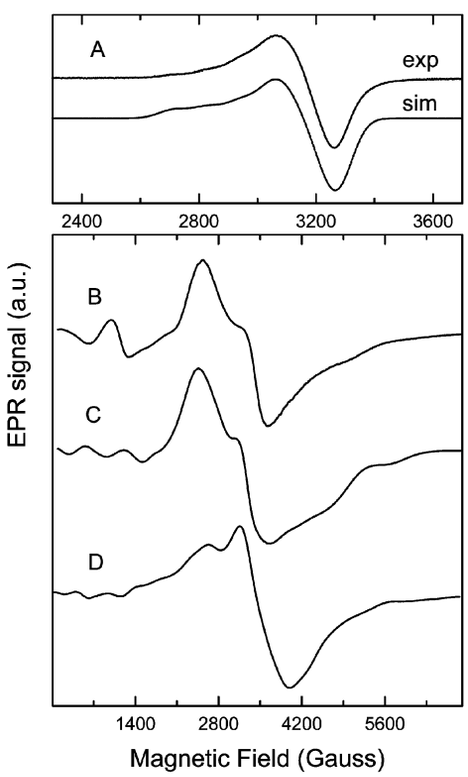


**Fig. 8** Experimental and simulated EPR spectra for a polycrystalline sample of **4** (A). EPR simulation parameters: $g_1 = 2.080$ (100 G), $g_2 = 2.158$ (140 G), and $g_3 = 2.350$, $A_3 = 10^{-2}$ cm$^{-1}$ (100 G) (linewidth within parentheses). *A*- and *g*-tensors were assumed to be coaxial. Experimental conditions: microwave frequency, 9.49 MHz; temperature, 15 K; Modulation, 5 G; microwave power, 0.2 mW. EPR spectra obtained for polycrystalline samples of **5** (B), **3** (C), and **1** (D). Experimental conditions: as for **4**, except temperature, 5 K.

The spectrum shown in Fig. 8A is a typical axial spectrum as observed in most Cu(II) ion complexes having square planar coordination. Simulation of this spectrum assuming axial symmetry yielded the EPR parameters $g_{||} = 2.35$, $A_{||} = 10^{-2}$ cm$^{-1}$ (100 G), and $g_\perp = 2.11$ (160 G) (linewidth in parentheses). The quadruple hyperfine splitting due to the Cu(II) nucleus ($I = 3/2$) is seen at $g_{||}$, but no hyperfine structure is resolved at $g_\perp$. On the other hand, as shown in Fig. 8A, the spectrum can be simulated assuming three different *g*-values ($g_1 = 2.08$, $g_2 = 2.16$, and $g_3 = 2.35$). The EPR parameters obtained assuming axial symmetry are unusual for Cu(II) ion compounds having square planar coordination and do not reflect the symmetry of the coordination site in **4**. Therefore, we favour the second set of EPR parameters to be more appropriate to explain the electronic properties of the Cu(II) ions in **4** since the crystal data shows a highly distorted Cu(II) ion site, with a coordination polyhedron which can be defined as a highly distorted octahedron toward a trigonal prism, as described above. However, the deviation of the *g*-values from axial symmetry is not so pronounced, suggesting that the main contribution to the Cu(II) ground state should be given by the $d_{x^2-y^2}$ orbital.[41] Evaluation of both *g*- and *A*-tensors in single crystal samples is necessary to elucidate this point. The fact that compound **4** shows resolved hyperfine structure indicates that exchange interactions among Cu(II) ions are negligible. This is in line with the magnetic behaviour of this compound, which follows the Curie law. Resolved hyperfine structure is usually observed only in frozen solution samples or powdered samples of Cu(II) compounds diluted in a diamagnetic matrix, where the magnetic interactions among copper centres are negligible. This does not happen in the solid state, where the magnetic interactions may produce broadening, narrowing and/or collapse of the EPR resonances.[39,40] This means that the intermolecular exchange interaction coupling constant *J* between Cu(II) ions, which is responsible for the collapse of the hyperfine structure, is smaller than $10^{-2}$ cm$^{-1}$ ($J < A$).

**Compounds 1, 3 and 5.** Figs. 8B, C, and D show the EPR spectra obtained for polycrystalline samples of compounds **5**, **3** and **1**, respectively. The spectra in solution are similar to those in the solid state (not shown), with broader resonance lines which likely originate from magnetic interactions among metallic clusters. Therefore, it can be concluded that the structure of the metallic clusters are kept in solution for compounds **3** and **5**, as observed for compound **4**.

The coordination around the Gd(III) ion is the same in compounds **3** and **5** (eight-coordination with a monodentate nitrate anion and a coordination polyhedron described as a distorted dodecahedron), and quite similar to that in compound **1** (nine-coordination with a bidentate nitrate anion and a coordination polyhedron described as a distorted monocapped dodecahedron). Since the coordination geometry of the Gd(III) ions is similar in the three compounds, one should expect similar Gd(III) EPR signals in all the compounds assuming that the Gd(III) ions are magnetically isolated in the crystal lattice. However, as seen in Fig. 8, they are different. For a magnetically uncoupled Gd(III) ion ($4f^7$, $S = 7/2$), a central line with $g \sim 2$ (transition $+1/2 \leftrightarrow -1/2$) and three lateral lines at both sides of the central line (transitions $\pm7/2 \leftrightarrow \pm5/2$, $\pm5/2 \leftrightarrow \pm3/2$, $\pm3/2 \leftrightarrow \pm1/2$) are expected.[42] In this context, the EPR spectrum of the Gd–Zn cryptate **5** (Fig. 8B), would arise solely from the Gd(III) ion since Zn(II) is diamagnetic: a single broad central line is observed, which is not centered at $g = 2.00$. The extra lines observed on both sides of the central line, which are not six as expected, may be attributed to the zero field splitting resonances. Therefore, the differences observed among the spectra may be associated either with the presence of the second metal ion in the cluster, Cu(II) in **3** and Gd(III) in **1**, or intercluster interactions (less likely).[43] Unfortunately, the complexity of the spectra shown in Figs. 8B, C, and D prevents a simple analysis. Additional work, such as single crystal EPR measurements, might help to understand the EPR properties of these compounds.

## Conclusions

The anionic azacryptand $(L^1 - 3H)^{3-}$ is able to form bimetallic cryptates with either two Ln(III) ions or one Ln(III) ion and one Cu(II) or Zn(II) ion. The X-ray crystal structures of the bimetallic cryptates show that the ligand is hellically wrapped around both metal ions. In the solid state the conformation of the cations $[Ln_2(L - 3H)(NO_3)_2]^+$ (Ln = Gd, Tb) is $\Lambda(\delta\delta\lambda)_5(\delta\delta\lambda)_5$ or its enantiomeric form $\Delta(\lambda\lambda\delta)_5(\lambda\lambda\delta)_5$, while for $[LnCu(L - 3H)(NO_3)]^+$ (Ln = Gd, Lu) it can be described as $\Lambda(\delta\delta\lambda)_5$-$(\delta'\delta'\delta')_5$ (or $\Delta(\lambda\lambda\delta)_5(\lambda'\lambda'\lambda')_5$). The magnetic behaviour of the homodinuclear (Gd, Gd) and the heterobinuclear (Gd, Cu) cryptates reveals the capability of the ligand to induce a significant magnetic interaction between the two metal ions. A quantitative analysis can be performed on the basis of a spin-only expression derived from the isotropic spin Hamiltonian $\boldsymbol{H} = -JS_{Gd1}S_{Gd2}$ (**1**) and $\boldsymbol{H} = -JS_{Cu}S_{Gd}$ (**3**). This magnetic interaction is antiferromagnetic in the case of the Gd–Gd cryptate, but ferromagnetic for the Gd–Cu one. The antiferromagnetic coupling observed for **1** is one of the largest ever reported. Although weak, the ferromagnetic coupling found in **3** is considerably stronger than the one reported for $[GdCu(L^2 - 3H)(DMF)](ClO_4)_2 \cdot MeCN$.[27] Analysis of the magnetic and structural data of these cryptates indicates that the bending of the bridging network, an essential feature directing the magnetic interaction, could be controlled by, for instance, substitution of the nitrate anion by a more bulky mono- or bidentate ligand. This opens new prespectives for the design of Gd(III)–Cu(II) compounds with more effective magnetic interactions. Finally, in spite of the similar coordination environment of the Gd(III) ion in compounds **1**, **3** and **5**, their EPR spectra are different, thereby suggesting that the changes are provoked by magnetic interactions between the Gd(III) ion and the Cu(II) ion in **3** and the other Gd(III) ion in **1**.

## Acknowledgements

We thank H. Adams for the X-ray crystal data collection of compound **2**. F. A., R. R-C, C. P-I., A. de B. and T. R-B. thank the Ministerio de Ciencia y Tecnología and FEDER (BQU2001-0796) for financial support and J.-C. G. B. the Swiss national science foundation. This research was performed within the framework of the EU COST Action D18 "Lanthanide Chemistry for Diagnosis and Therapy".

## References

1 J.-C. G. Bünzli, in *Rare Earths*, eds. R. Saez-Puche and P. Caro, Editorial Complutense, Madrid, 1998, p. 223ff.
2 A. E. Merbach and É. Tóth, *The Chemistry of Contrast Agents in Medical Magnetic Resonance Imaging*, John Wiley & Sons, Chichester, 2001.
3 J. A. Peters, J. Huskens and D. J. Raber, *Prog. Magn. Reson. Spectrosc.*, 1996, **28**, 283.
4 A. Roigk, R. Hettich and H.-J. Schneider, *Inorg. Chem.*, 1998, **37**, 751.
5 G. L. DeNardo, G. R. Mirik, L. A. Kroger, R. T. O'Donnel, C. F. Meares and S. L. DeNardo, *J. Nucl. Med.*, 1996, **37**, 451.
6 G. Mathis, in *Rare Earths*, eds. R. Saez-Puche and P. Caro, Editorial Complutense, Madrid, 1998, pp. 285–297.
7 J.-C. G. Bünzli and C. Piguet, *Chem. Rev.*, 2002, **102**, 1897–1928.
8 J.-P. Costes, F. Dahan, B. Donnadieu, J. García-Tojal and J.-P. Laurent, *Eur. J. Inorg. Chem.*, 2001, 363; J.-P. Costes, F. Dahan, A. Dupuis and J.-P. Laurent, *Chem. Eur. J.*, 1998, **4**, 1616.
9 J.-P. Costes, F. Dahan and A. Dupuis, *Inorg. Chem.*, 2000, **39**, 165.
10 J.-P. Costes, F. Dahan, A. Dupuis and J.-P. Laurent, *Inorg. Chem.*, 2000, **39**, 169.
11 T. Sanada, T. Suzuki, T. Yoshida and S. Kaizaki, *Inorg. Chem.*, 1998, **37**, 4712.
12 J.-P. Costes, J. M. Clemente-Juan, F. Dahan, F. Nicodème and M. Verelst, *Angew. Chem., Int. Ed.*, 2002, **41**, 323.
13 R. Hedinger, M. Ghisletta, K. Hegetschweiler, É. Tóth, A. E. Merbach, R. Sessoli, D. Gatteschi and V. Gramlich, *Inorg. Chem.*, 1998, **37**, 6698.
14 E. Baraniak, R. ST. L. Bruce, H. C. Freeman, N. J. Hair and J. James, *Inorg. Chem.*, 1976, **15**, 2226.
15 X.-M. Chen, Y.-L. Wu, Y.-X. Tong, Z. Sun and D. N. Hendrickson, *Polyhedron*, 1997, **16**, 4265.
16 M. Sakamoto, K. Manseki and H. Okawa, *Coord. Chem. Rev.*, 2001, **379**, 219–221.
17 J.-P. Costes, F. Dahan, A. Dupuis, S. Lagrave and J.-P. Laurent, *Inorg. Chem.*, 1998, **37**, 153.
18 M. G. B. Drew, O. W. Howarth, C. J. Harding, N. Martin and J. Nelson, *J. Chem. Soc., Chem. Commun.*, 1995, 903.
19 F. Avecilla, R. Bastida, A. de Blas, D. E. Fenton, A. Macías, A. Rodríguez, T. Rodríguez-Blas, S. García-Granda and R. Corzo-Suárez, *J. Chem. Soc., Dalton Trans.*, 1997, 409.
20 C. Platas, F. Avecilla, A. de Blas, C. F. G. C. Geraldes, T. Rodríguez-Blas, H. Adams and J. Mahía, *Inorg. Chem.*, 1999, **38**, 3190.
21 C. F. G. C. Geraldes, S. Zhang, C. Platas, T. Rodríguez-Blas, A. de Blas and A. D. Sherry, *J. Alloys Compd.*, 2001, **824**, 323–324.
22 C. Platas, F. Avecilla, A. de Blas, T. Rodríguez-Blas, C. F. G. C. Geraldes, É. Tóth, A. E. Mebach and J.-C. G. Bünzli, *J. Chem. Soc., Dalton Trans.*, 2000, 611.
23 F. Avecilla, A. de Blas, R. Bastida, D. E. Fenton, J. Mahía, A. Macías, C. Platas, A. Rodríguez and T. Rodríguez-Blas, *Chem. Commun.*, 1999, 125.
24 Q.-Y. Chen, Q.-H. Luo, Z.-L. Wang and J.-T. Chen, *Chem. Commun.*, 2000, 1033.
25 Q.-Y. Chen, Q.-H. Luo, L.-M. Zheng, Z.-L. Wang and J.-T. Chen, *Inorg. Chem.*, 2002, **41**, 605.
26 R. Rodríguez-Cortiñas, F. Avecilla, C. Platas-Iglesias, D. Imbert, J.-C. G. Bünzli, A. de Blas and T. Rodríguez-Blas, *Inorg. Chem.*, 2002, **41**, 5336.
27 Q.-Y. Chen, Q.-H. Luo, D.-G. Fu and J.-T. Chen, *J. Chem. Soc., Dalton Trans.*, 2002, 2873.
28 L. N. Mulay, in *Theory and Applications of Molecular Magnetism*, eds. E. A. Boudreaux and L. N. Mulay, John Wiley & Sons, New York, 1976, pp. 491–495; R. R. Gupta, in *Landolt-Börnstein New Series, Numerical and Functional Relationships in Science and Technology*, ed. O. Madelung, *Group II: Atomic and Molecular Physics*, vol. 16, *Diamagnetic Susceptibility*, Springer-Verlag, Berlin, Heidelberg, 1986.
29 G. M. Sheldrick, SHELXTL Bruker Analytical X-ray System, release 5.1, Madison, WI, 1997.
30 G. Bernardelli and H. D. Flack, *Acta Crystallogr., Sect. A*, 1985, **41**, 500.
31 M. Elhabiri, R. Scopelliti, J.-C. G. Bünzli and C. Piguet, *J. Am. Chem. Soc.*, 1999, **121**, 10747.
32 A. Panagiotopoulos, T. F. Zafiropoulos, S. P. Perlepes, E. Bakalbassis, I. Masson-Ramade, O. Kahn, A. Terzis and C. P. Raptopoulou, *Inorg. Chem.*, 1995, **34**, 4918.
33 W. Plass and G. Fries, *Z. Anorg. Allg. Chem.*, 1997, **623**, 1205.
34 J.-P. Costes, A. Dupuis and J.-P. Laurent, *Inorg. Chim. Acta*, 1998, **268**, 125.
35 P. Guerriero, S. Tamburini, P. A. Vigato and C. Benelli, *Inorg. Chim. Acta*, 1991, **189**, 19.
36 S. Liu, L. Gelmini, S. J. Rettig, R. C. Thompson and C. Orvig, *J. Am. Chem. Soc*, 1992, **114**, 6081.
37 J.-P. Costes, F. Dahan, A. Dupuis and J.-P. Laurent, *New J. Chem.*, 1998, **22**, 1525; J.-P. Costes, F. Dahan, A. Dupuis and J.-P. Laurent, *Inorg. Chem.*, 1997, **36**, 3429; J.-P. Costes, F. Dahan, A. Dupuis and J.-P. Laurent, *Inorg. Chem.*, 1996, **35**, 2400; A. Bencini, C. Benelli, A. Caneschi, R. L. Carlin, A. Dei and D. Gatteschi, *J. Am. Chem. Soc.*, 1985, **107**, 8128; A. Bencini, C. Benelli, A. Caneschi, A. Dei and D. Gatteschi, *Inorg. Chem.*, 1986, **25**, 572; N. Matsumoto, M. Sakamoto, H. Tamaki, H. Okawa and S. Kida, *Chem. Lett.*, 1990, 853; Sakamoto, M. Hashimura, K. Matsuki, N. Matsumoto, K. Inoue and H. Okawa, *Bull. Chem. Soc. Jpn.*, 1991, **64**, 3639; I. Ramade, O. Kahn, Y. Jeannin and F. Robert, *Inorg. Chem.*, 1997, **36**, 930; C. Benelli, A. J. Blake, P. E. Y. Milne, J. M. Rawson and R. E. P. Winpenny, *Chem. Eur. J.*, 1995, **1**, 614; A. Bouayad, C. Brouca-Cabarrecq, J. C. Trombe and A. Gleizes, *Inorg. Chim. Acta*, 1992, **195**, 193; A. J. Blake, P. E. Y. Milne, P. Thornton and R. E. P. Winpenny, *Angew. Chem., Int. Ed. Engl.*, 1991, **30**, 1139.
38 M. Andruh, I. Ramade, E. Codjovi, O. Guillou, O. Kahn and J.-C. Trombe, *J. Am. Chem. Soc.*, 1993, **115**, 1822.
39 C. D. Brondino, R. Calvo and E. J. Baran, *Chem. Phys. Lett*, 1997, **271**, 51–54.
40 A. Bencini and D. Gatteschi, *EPR of Exchange Coupled Systems*, Springer-Verlag, Berlin, 1990.
41 H. J. Zeiger and G. W. Pratt, *Magnetic Interactions in Solids*, Oxford University Press, London, 1973.
42 A. Abragam and B. Bleaney, *Electron Paramagnetic Resonance of Transition Ions*, Clarendon Press, Oxford, 1970.
43 C. Benelli and D. Gatteschi, *Chem. Rev.*, 2002, **102**, 2369–2387 and references therein.